Journal of
Synchrotron
Radiation

ISSN 0909-0495

Received 1 March 2010
Accepted 6 April 2010

A bi-prism interferometer for hard X-ray photons

A. F. Isakovic,[a,d] A. Stein,[a] J. B. Warren,[a] A. R. Sandy,[b] S. Narayanan,[b] M. Sprung,[b]‡ J. M. Ablett,[a]¶ D. P. Siddons,[a] M. Metzler[c] and K. Evans-Lutterodt[a]*

[a]Brookhaven National Laboratory, Upton, NY 11973, USA, [b]X-ray Science Division, Argonne National Laboratory, Argonne, IL 60439, USA, [c]Cornell NanoScale Science and Technology Facility, Ithaca, NY 14850, USA, and [d]Khalifa University of Science, Technology and Research, Abu Dhabi, UAE. E-mail: kenne@bnl.gov

Micro-fabricated bi-prisms have been used to create an interference pattern from an incident hard X-ray beam, and the intensity of the pattern probed with fluorescence from a 30 nm-thick metal film. Maximum fringe visibility exceeded 0.9 owing to the nano-sized probe and the choice of single-crystal prism material. A full near-field analysis is necessary to describe the fringe field intensities, and the transverse coherence lengths were extracted at APS beamline 8-ID-I. It is also shown that the maximum number of fringes is dependent only on the complex refractive index of the prism material.

© 2010 International Union of Crystallography
Printed in Singapore – all rights reserved

Keywords: interferometers; prisms; coherence.

1. Introduction

The prism as an optical element for hard X-ray photons was introduced over 70 years ago, for example in attempts to determine the ratio *e*/*m* (Stauss, 1930). However, the limited useful aperture results in hard X-ray prisms (HXPs) being seldom used, in contrast with the many applications of visible-light prisms. The limited aperture results from the small deflection angles possible with refraction at a single interface, combined with a relatively large absorption coefficient. Based on the wide array of uses for visible-light prisms, it is clear that HXPs could have a significant impact in a variety of fields such as X-ray interferometry, holography and phase-contrast microscopy. For example, interferometric methods can be the basis of precision measurements of the refractive index at these hard X-ray photon energies (Rosfjord *et al.*, 2006; Leitenberger *et al.*, 2001). We have fabricated arrays of silicon bi-prisms with standard micro-fabrication methods, and have used them to implement interferometers with which we have measured the transverse coherence lengths of beamline 8-ID-I at the APS.

Flexible ways to obtain interference patterns sensitive to the transverse coherence length for hard X-ray photons are of great current interest (Snigirev *et al.*, 2009; Suzuki, 2004; Weitkamp *et al.*, 2005; Momose *et al.*, 1998; Lang & Makepeace, 1999), but there have been relatively few successful examples. A natural way to obtain interference patterns is to perform a Young's double-slit (YDS) experiment. In this approach a pair of pinholes is illuminated by a beam, where the visibility of the interference fringes can be correlated to the transverse coherence of the beam. Although conceptually simple, it is difficult to implement the ideal YDS experiment for photons in the hard X-ray spectrum. The pinholes must be small ($\sim 10^{-6}$ m), yet the film needs to be sufficiently thick ($\sim 10^{-4}$ m) to attenuate all photons not passing through the pinholes. The resulting large aspect ratio of film thickness to pinhole diameter ($\sim 10^{-4}\,\text{m}/10^{-6}\,\text{m} = 10^{2}$) is difficult to fabricate. Even if fabrication is successful, the aspect ratio of the pinhole (Fuhse & Salditt, 2006) is such that the pair of pinholes may be more accurately modeled as two weakly coupled waveguides, a more complicated system to analyze than the simple YDS model. In spite of these difficulties, the pinhole YDS experiment was employed successfully at lower photon energies (Liu *et al.*, 2001; Leitenberger *et al.*, 2004). However, as the experiment (Leitenberger *et al.*, 2004) showed, at the higher energies the film becomes more transparent, and the classic YDS pattern is overwhelmed by interference between each pinhole separately with the transmission through the film.

2. Method

We chose instead to implement a hard X-ray bi-prism interferometer (HXBI) by micro-fabricating bi-prisms, examples of which are shown in Figs. 1(*a*) and 1(*b*). In this approach, light is deflected by an angle θ_T by a pair of prisms to a region of overlap where a fringe pattern is generated, as depicted in Fig. 1(*c*). The refracting surface has an angle θ_P with respect to the *x*-axis. The effect of each prism is to create a separate virtual source, and one can view the resulting fringe field as originating from the interference owing to the two virtual sources, *i.e.* a virtual YDS. In this wavefront-division method,

‡ Currently at HASYLAB, Hamburg, Germany.
¶ Currently at SOLEIL, Gif sur Yvette, France.

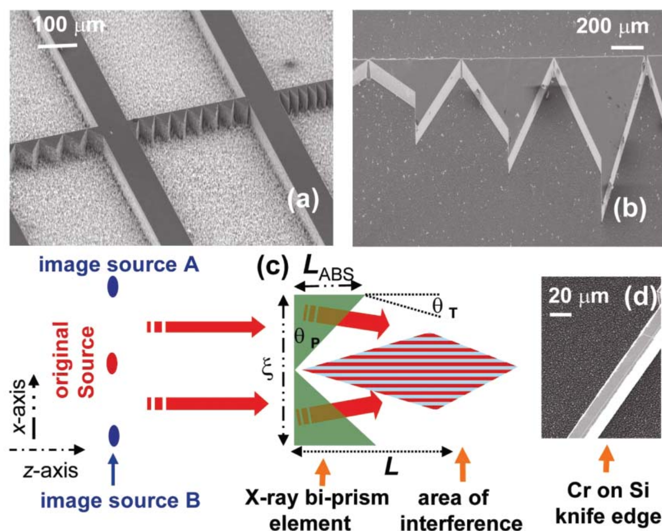

Figure 1
(*a*) Top view of a one-dimensional array of X-ray prisms, nanofabricated from Si, with varying prism angle in each channel. (*b*) The second family of prisms used in this study. (*c*) Schematic (not to scale) of the experiment, illustrating the creation of a pair of virtual sources from a single real source. (*d*) SEM image of the Cr-capped Si wall that serves as the 'knife edge' for X-ray fluorescence.

the transverse coherence length ξ sets an upper bound on the useful size of the prism that produces interference fringes. The number of fringes at the maximal overlap distance L from the prism ($L \simeq \xi/2\theta_T$) is given by $N \simeq \xi/(\lambda/2\theta_T)$. In order to get at least one fringe, one finds that $\theta_T > \lambda/2\xi$. This implies that $L < \xi^2/\lambda$, and consequently all fringes obtained with this bi-prism method are going to be in the near-field Fresnel regime, not the far-field Fraunhofer regime, as is the case of the conventional YDS. The maximum number of fringes is constrained by absorption in the prism as we now show. The deflection owing to a single prism is given by $\theta_T \simeq \delta\tan(\theta_P)$. For a transverse coherence length ξ, the maximum useful θ_P of the prism is set by $\tan(\theta_P) = L_{ABS}/(\xi/2)$, where L_{ABS} is the absorption length and equals $\lambda/(4\pi\beta)$. Thus $\tan(\theta_P) < \lambda/(2\pi\beta\xi)$ and one can show that the number of fringes in the maximal overlap region $N_{max} < \delta/(4\pi\beta)$, and this is dependent only on the ratio of the real and imaginary parts of the refractive index of the prism material. Tabulated Si values for δ and β give between 1 and 15 fringes for energies between 5 and 15 keV, which we show is in a very good agreement with the interference patterns presented here. Outside this overlap region fringes are strongly attenuated.

We micro-fabricated bi-prisms in silicon (Si) with angles that ranged from 25° to 80°, with details discussed elsewhere (Stein *et al.*, 2008; Isakovic *et al.*, 2008; Ablett *et al.*, 2004) except that 30 nm chromium (Cr) film is used in place of SiO_2 film. Measurements were performed at APS beamline 8-ID-I and relevant details of the beamline have already been documented (Sandy *et al.*, 2007). Some measurements were also performed at NSLS beamline X13B. Although the simplest method for visualizing the fringes is to use a scintillator viewed by a microscope and CCD camera, the resulting data are significantly degraded by the optical resolution of the combination and scattered light, resulting in smeared low-contrast fringes. We used such a system for initial alignment, but for quantitative measurements we directly measured the fringes with X-ray fluorescence (XRF) from a metal strip. A Si wall, several hundred micrometers long and about 40 μm high, was micro-fabricated, and capped with a 30 nm-thick layer of Cr film that served as a very thin wire-like probe (Fig. 1*d*). An '$xyz\theta_x\theta_y$' micro-translating stage controlled the positioning of a small Si wafer bearing this probe, and a VORTEX detector (SII_NanoTechnology, http://www.siint.com/en/products/vortex/vortex.html) was sited about 8 cm away from the probe, in a near-perpendicular orientation to the direction of propagation of the X-ray beam. Since the Cr strip was extended along the beam direction, it needed to be oriented with respect to the fringes to maximize the resolution (*i.e.* minimize its projected width). Slits upstream of the prism restricted X-rays to illuminate the active prism areas, typically 200 μm × 40 μm or smaller when required to illuminate a single biprism. The data could be normalized by measuring the field intensity present after translating the prism out of the path.

3. Results and discussion

We show the fringes as a function of three variables, the prism angle in Fig. 2, the photon energy in Figs. 3(*a*)–3(*c*), and distance from prism in Figs. 3(*d*)–3(*f*). Besides observation of a fringe intensity profile with the expected fringe period given

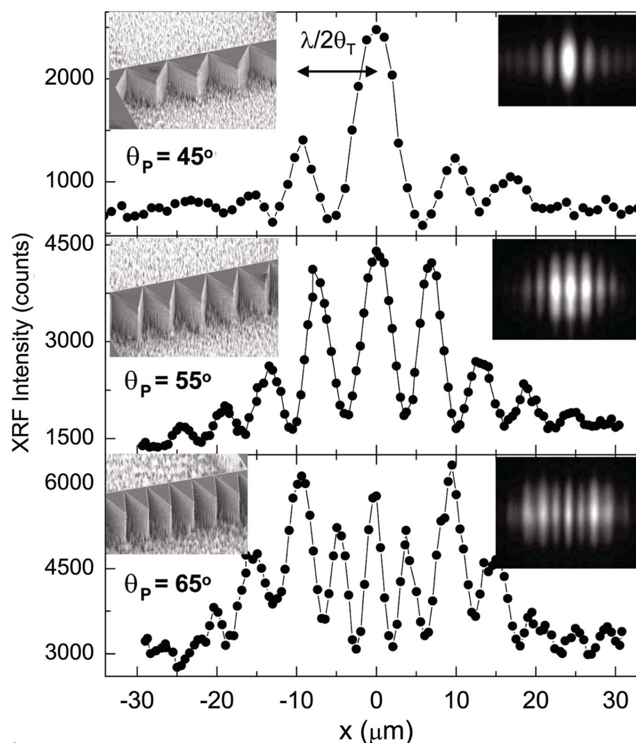

Figure 2
(Top to bottom) Evolution of the interference pattern with changing prism angle. Left-hand insets are SEM images of prisms, while the right-hand insets are YAG/CCD images of the corresponding interference patterns.

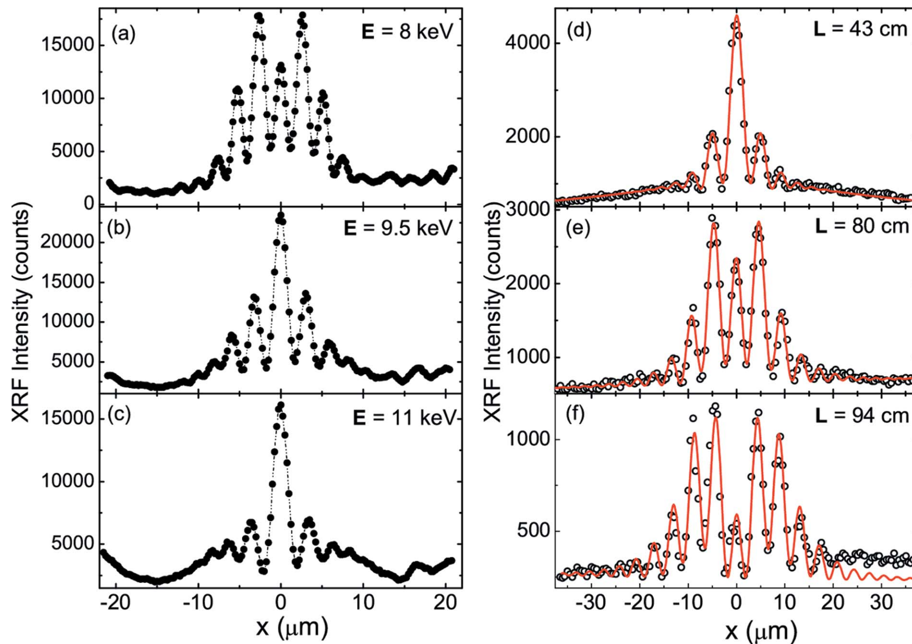

Figure 3
(*a*)–(*c*) Evolution of the interference pattern with X-ray photon energy. The line is a guide to the eye. (*d*)–(*f*) Evolution of the fringe patterns as a function of the separation between the 65° prism from Fig. 1(*b*) and the Cr 'knife edge'. The red line is a fit, based on the model presented in the text.

by $\lambda/2\theta_T$, what is immediately striking about the data in Figs. 2 and 3 is the non-monotonic behavior of the intensities of the fringes, which we address in the next paragraph. Some other aspects of the fringe pattern are more readily interpreted, including the dependence on the prism angle and the energy dependency. For example, at a fixed distance of the Cr strip from the bi-prism, larger prism angles θ_P result in larger deflection angles $\theta_T \simeq \delta\tan(\theta_P)$, and this gives a larger region for fringe overlap and a smaller period L_P for the fringes, where $L_P = \lambda/(2\theta_T)$, as shown in Fig. 2. In Figs. 3(*a*)–3(*c*) we show intensity as a function of photon energy for fixed prism angle (65°), illustrating that the deflection angle θ_T and the overlap region decrease with increasing energy, while L_P is increasing with increasing energy. Conventional optical YDS experiments have a smoothly varying fringe intensity envelope function. The lack of smoothly varying envelope here is a direct result of being in the Fresnel regime. To accurately describe this we have generated a non-linear least-squares fitting procedure based on the Fresnel–Kirchoff diffraction formula. If one makes the usual approximation of a 'thin' optic (Goodman, 1996), one has an equation of the form

$$U(x,z) = \frac{1}{i\lambda}\int T(\eta)\frac{\exp(ikr_{01})}{r_{01}}\,\mathrm{d}\eta, \qquad (1)$$

where $k = 2\pi/\lambda$ and $r_{01} = [z^2 + (x-\eta)^2]^{1/2}$, with (x, z) defining the image plane at a distance z from the prism and the variable η is in the 'thin' object plane. We model the prisms as a thin optic with a transmission function with phase shift and amplitude given by $T(\eta) = \exp\{-[2\pi\beta t(\eta)]/\lambda\}\exp\{i[2\pi\delta t(\eta)]/\lambda\}$, where $t(\eta) = \mathrm{abs}(\eta)\tan(\theta_P)$ represents the thickness of the prism, and η is the distance from the optical axis.

One can qualitatively understand the unexpected envelope of intensities. If one illuminates either prism of the bi-prism pair separately, one obtains the familiar modulated intensity pattern owing to coherent illumination of an aperture (Goodman, 1996), except that there is an apparent shift of the source. The illumination of both prisms of the bi-prism pair results in the interference fringes, but these fringe intensities are modified by the product of the aforementioned modulation functions. The resulting fringe intensities thus depend on the distance from the bi-prism; and this is most clearly visible in the experimental data presented in Figs. 3(*d*)–3(*f*), where the fringe intensities are shown at different distances from the prism. The quality of the overlap between the model and raw XRF data in Fig. 3 further supports this picture.

Given this demonstration of a practical hard X-ray interferometer, a natural experiment is to attempt to determine the transverse coherence length in a beamline, which in the ideal case is due only to the source size and distance from the source. In practice, a beamline often has imperfect optical components that will degrade the beam coherence. At the APS 8-ID-I beamline the 'one sigma' source sizes are quoted to be 11 μm in the vertical and 110 μm in the horizontal. Figs. 4(*a*) and 4(*b*) show the resulting fringe intensity profile in the vertical and horizontal directions. One can see immediately that the vertical orientation displays greater fringe visibility and contrast than does the horizontal profile, showing qualitatively that the source size in the vertical is smaller than in the horizontal. In Fig. 4(*c*) the extracted non-uniform fringe visibility emphasizes the near-field behavior. The maximum fringe visibilities in the vertical are above 0.9, and are ~0.6 in the horizontal.

We extracted the asymmetric source size from the fit to the data points using our model described above, where the source is modeled as a completely incoherent source of a Gaussian line-shape. We combined this with $T(\eta)$ defined above and numerically integrated over the Gaussian source in order to generate the line-shape that was fit to the data. From the fits we extracted a vertical source size of 10 ± 5 μm and a horizontal source size of 130 ± 20 μm. These measured source sizes were comparable with the quoted source sizes above, implying that the beamline preserves the coherence of the source quite well in both directions, but is slightly worse in the horizontal direction.

In the YDS, the fringe visibility is uniform and is directly related to the complex coherence factor μ_{12} (Goodman, 1985). In order for the fringe visibility to be equal to μ_{12}, the intensity from each aperture should be equal, which is not the

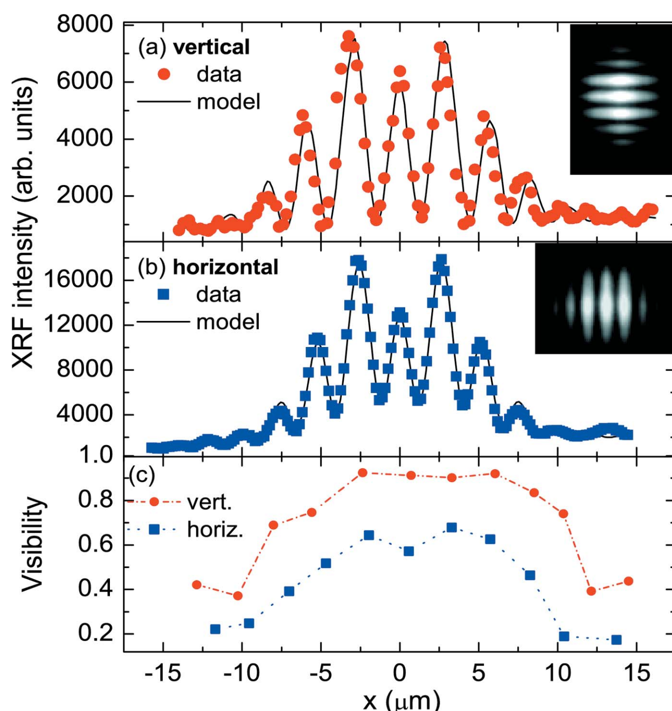

Figure 4
(*a*) X-ray interference pattern for a vertical orientation of the X-ray bi-prism. The fit, obtained numerically as described in the text, is a solid line. (*b*) The same type of measurement and the fit for the horizontal orientation. The right-hand insets in (*a*) and (*b*) are CCD interference patterns. (*c*) Lateral spatial variation of the visibility factor for two mutually perpendicular positions of the X-ray bi-prism optics.

case here. Symmetry suggests that the central fringe is likely to have equal amplitude from both prisms independent of any details, and should allow its use as a semi-quantitative guide to make comparisons.

We list some of the advantages of using micro-fabricated bi-prisms for an X-ray interferometer, in combination with the XRF method for quantifying the interference fringe intensities. The simplicity of the system allows one to model the measured fringe intensities from first principles. The bi-prism can function as an interferometer over a wide range of energies, by simply increasing the detector distance to compensate for the reduced deflection angles at higher energies. The lithographic methods for defining the bi-prisms allow a phase accuracy of order (50 nm/30 μm) $\times 2\pi \simeq 5 \times 10^{-3}\pi$ owing to 50 nm placement accuracy. Imperfections can be quantified with a scanning electron microscope (SEM) and included in the modeling of the system, as modifications to $T(\eta)$. The useful signal is not limited to the flux that passes through sub-micrometer pinholes, and consequently the HXBI will have improved signal-to-noise ratio over YDS. Using the 30 nm thin metal film as a detector allows one to quantify the fringe intensities with fringe periods as small as 60 nm; thinner metal films should allow detection of fringe periods down to the 5 nm range. This interferometer is more sensitive to the transverse rather than the longitudinal coherence length. The bandwidth of the monochromator at 8-ID-I is of the order of 2 eV, giving a longitudinal coherence of ∼0.5 μm. For typical deflection angles of $\sim 10^{-5}$, a longitudinal coherence length of 0.5 μm will not affect the data shown here.

Real sources may be partially spatially coherent, and a more complete description of the source will be the measured complex coherence factor μ_{12} (Goodman, 1985). For the classical YDS, μ_{12} can be extracted from the dependence of the fringe visibility as a function of separation between the slits. For this bi-prism interferometer, a direct route to extraction of μ_{12} can be deduced from an extension of Schell's theorem (Nugent, 1990), which applies even in the near-field limit, which is the case here.

4. Conclusion

Using micro-fabricated prisms we have implemented a bi-prism interferometer for hard X-ray photons. We measured the absolute amplitude of the fringes from the XRF signal from a 30 nm Cr metal film scanned through the fringe field. Unlike the classical far-field Fraunhofer analysis typically adopted, we found that Kirchhoff–Fresnel near-field analysis needs to be applied for the X-ray bi-prism method at hard X-ray wavelengths. The number of fringes in the classical overlap region is comparable to $\delta/(4\pi\beta)$, the ratio of real to imaginary parts of the refractive index of the prism material, showing a path towards better interferometers. We have shown that for typical monochromatic bandwidths this interferometer is more sensitive to transverse than longitudinal coherence lengths. Finally, we measured the transverse coherence lengths of the APS 8-ID-I beamline. These results suggested that micro-fabricated prisms will play a larger role in novel hard X-ray optical arrangements for phase-contrast methods and other types of interferometeric imaging and characterization.

Use of the NSLS, the CFN and the NSLS-II project at BNL was supported by the US DOE, Office of Basic Energy Sciences, under Contract No. DE-AC02-98CH10886, and the use of ANL-APS is supported through the DOE contract DE-AC02-06CH11357. This work was performed in part at the Cornell CNF, a member of NNIN, which is supported by the NSF. AFI and KEL acknowledge early support through BNL LDRD 06-046, P. Takacs (BNL) for early suggestions about the manuscript, and C. C. Kao (BNL) for support. We thank G. Bordonaro and R. Ilic of CNF for timely technical assistance.

References

Ablett, J. M., Evans-Lutterodt, K. & Stein, A. (2004). *Proc. SPIE*, **5539**, 88–94.
Fuhse, A. & Salditt, T. (2006). *Opt. Commun.* **265**, 140–146.
Goodman, J. W. (1985). *Statistical Optics.* New York: Wiley.
Goodman, J. W. (1996). *Introduction to Fourier Optics.* Stanford University: McGraw-Hill.
Isakovic, A. F., Evans-Lutterodt, K., Stein, A., Elliot, D. & Warren, J. B. (2008). *J. Vac. Sci. Technol. A*, **26**, 1182.
Lang, A. R. & Makepeace, A. P. W. (1999). *J. Synchrotron Rad.* **6**, 59–61.

Leitenberger, W., Kuznetsov, S. M. & Snigirev, A. (2001). *Opt. Commun.* **191**, 91–96.
Leitenberger, W., Wendrock, H., Bischoff, L. & Weitkamp, T. (2004). *J. Synchrotron Rad.* **11**, 190–197.
Liu, Y., Seminario, M., Tomasel, F. G., Chang, C., Rocca, J. J. & Attwood, D. T. (2001). *Phys. Rev. A*, **63**, 033802.
Momose, A., Takeda, T., Itai, Y., Yoneyama, A. & Hirano, K. (1998). *J. Synchrotron Rad.* **5**, 309–314.
Nugent, K. A. (1990). *Opt. Commun.* **79**, 267–269.
Rosfjord, K., Chang, C., Miyakawa, R., Barth, H. & Attwood, D. T. (2006). *Appl. Opt.* **45**, 1730–1736.
Sandy, A. R., Evans-Lutterodt, K., Fezzaa, K., Kim, S., Narayanan, S., Sprung, M. & Stein, A. G. (2007). *Proc. SPIE*, **6705**, 67050N.
Snigirev, A., Snigireva, I. & Kohn, V. (2009). *Phys. Rev. Lett.* **103**, 064801.
Stauss, H. E. (1930). *Phys. Rev.* **36**, 1101–1108.
Stein, A., Evans-Lutterodt, K., Bozovic, N. & Taylor, A. (2008). *J. Vac. Sci. Technol. B*, **26**, 122–127.
Suzuki, Y. (2004). *Rev. Sci. Instrum.* **75**, 1026.
Weitkamp, T., Diaz, A., David, C., Pfeiffer, F., Stampanoni, M., Cloetens, P. & Ziegler, E. (2005). *Opt. Express*, **13**, 6296–6304.